Elimination of LWD (Logging While Drilling) Tool Modes Using Seismoelectric Data

Xin Zhan[1,*], Zhenya Zhu[1], Shihong Chi[2] and M. Nafi Toksöz[1]

[1] *Earth Resources Laboratory, Massachusetts Institute of Technology, Building 54-1815, 77 Massachusetts Ave, Cambridge, MA 02142, USA.*
[2] *Petrophysics, ConocoPhillips, 600 North Dairy Ashford, Houston, TX 77252, USA.*

Abstract. Borehole acoustic logging-while-drilling (LWD) for formation evaluation has become an indispensable part of hydrocarbon reservoir assessment [F. Cittá, C. Russell, R. Deady and D. Hinz, The Leading Edge, 23 (2004), pp. 566-573]. However, the detection of acoustic formation arrivals over tool mode contamination has been a challenging problem in acoustic LWD technology. In this paper we propose a new method for separating tool waves from formation acoustic waves in acoustic LWD. This method is to measure the seismoelectric signal excited by the LWD acoustic waves. The LWD tool waves which propagate along the rigid tool rim can not excite any electric signal. This is due to the effectively grounding of the drill string during the LWD process makes it impossible to accumulate any excess charge at the conductive tool — borehole fluid interface. Therefore, there should be no contribution by the tool modes to the recorded seismoelectric signals. To theoretically understand the seismoelectric conversion in the LWD geometry, we calculate the synthetic waveforms for the multipole LWD seismoelectric signals based on Pride's theory [S. R. Pride, Phys. Rev. B, 50 (1994), pp. 15678-15696]. The synthetic waveforms for the electric field induced by the LWD-acoustic-wave along the borehole wall demonstrate the absence of the tool mode. We also designed the laboratory experiments to collect simulated LWD monopole and dipole acoustic and seismoelectric signals in a borehole in sandstone. By analyzing the spectrum of acoustic and electric signals, we can detect and filter out the difference between the two signals, which are the mainly tool modes and noise.

AMS subject classifications: 86-05, 86-08, 86A25, 76W05

Key words: Logging While Drilling, acoustoelectric logging, multipole LWD seismoelectric signal, laboratory experiment, numerical simulation.

*Corresponding author. *Email addresses:* `xinzhan@mit.edu` (X. Zhan), `zhenya@mit.edu` (Z. Zhu), `Shihong.Chi@conocophillips.com` (S. Chi), `toksoz@mit.edu` (M. N. Toksöz)

1   Introduction

When a fluid electrolyte comes into contact with a neutral solid surface, anions from the electrolyte are chemically absorbed to the wall leaving behind a net excess of cations distributed near the wall. The region is known as the electric double layer [8]. When acoustic waves propagate through a fluid-saturated porous medium, a relative fluid-solid motion is generated (the motion of pore fluid with respect to the solid matrix). This pore fluid relative motion in rocks will induce a streaming electric field due to the electrical charges concentrated in the electric double layer (EDL) [7, 9]. This electric field is a localized one induced by the pressure front of the propagating acoustic wave and posses the same appearant velocity as the acoustic wave [13].

Acoustic logging-while-drilling (LWD) technology was developed in the 1990's to meet the demand for real-time acoustic logging measurements for the purpose of providing seismic tie and acoustic porosity and pore pressure determination [2,6]. The LWD apparatus, with sources and receivers located close to the borehole wall and the drill collar taking up a large portion of the borehole, have some significant effects on borehole acoustic modes. The tool waves are strong in amplitude and always exist in the multipole LWD measurements. These and others noise sources contaminate the true formation acoustic waveforms, causing difficulty in the recognition of formation arrivals. The various vibrations of the drill string in its axial, radial, lateral, and azimuthal directions, together with the impact of the drill string on the borehole wall and the impact of the drill bit on the formation, generate strong drilling noise. Field measurements [4] have shown that the frequency range of this noise influences the frequency range of the measurement of shear wave velocities in slow formations. It is the difficulty in characterizing and removing the source of the noise that has motivated the research in this paper.

2   Theoretical and numerical simulations

We first theoretically develop a Pride-theory-based model for the LWD-acoustic-wave induced electric fields. In the numerical modeling, we could set the vanishing of the electric field at the LWD tool surface to be the boundary condition. This reveals the basic mechanism in the LWD seismoelectric conversion. The synthetic LWD electric waveforms also confirm the absence of tool modes, which is consistent with our experimental results.

2.1   Mathematical formulation of the converted electrical field in LWD borehole geometry

According to Pride's theory [9, 10], elastic field is coupled with the electromagnetic field. The coupling between the acoustic and electromagnetic field in a porous media can be

expressed by

$$J = \sigma E + L(-\nabla p + \omega^2 \rho_f u), \tag{2.1}$$

$$-i\omega w = LE + (-\nabla p + \omega^2 \rho_f u)\frac{\kappa}{\eta}, \tag{2.2}$$

where J is the total electric current density, E is the electric field strength, u is the solid frame displacement, w is the fluid filtration displacement and p is the pore fluid pressure. L is the coupling coefficient, ρ_f and η are the density and the viscosity of the pore fluid, κ and σ are the dynamic permeability and conductivity of the porous medium respectively, ω is the angular frequency. The detailed expressions of L, κ are given as follows:

$$\frac{\kappa(\omega)}{\kappa_0} = \left[\left[1 - i\frac{\omega}{\omega_c}\frac{4}{m} \right]^{\frac{1}{2}} - i\frac{\omega}{\omega_c} \right]^{-1},$$

$$\frac{L(\omega)}{L_0} = \left[1 - i\frac{\omega}{\omega_c}\frac{m}{4}\left(1 - 2\frac{\widetilde{d}^2}{\Lambda}\right)\left(1 - i^{\frac{3}{2}}\frac{\widetilde{d}}{\delta}\right)^2 \right]^{-\frac{1}{2}}, \tag{2.3}$$

where κ_0 is the Darcy permeability, $\omega_c = \varphi\eta/\alpha_\infty\kappa_0\rho_f$ is the transition frequency from viscous flow to inertial flow, α_∞ is tortuosity, m is a dimensionless parameter defined as $m = \phi\Lambda^2/\alpha_\infty\kappa_0$ and is assumed to be 8 in our calculation, Λ is the characteristic pore size, $\delta = \sqrt{\eta/\omega\rho_f}$ is the viscous skin depth, $\widetilde{d}$ is less than or equal to the Debye length d,

$$\widetilde{d} \leqslant d = \sqrt{\varepsilon_f k_B T/e^2 z^2 N}, \tag{2.4}$$

where ε_f is the fluid permittivity, k_B is the Boltzman constant, T is absolute temperature, e is the electric charge, z is the ionic valence of the solution, and N is ion concentration and defined as $N = 6.022 \times 10^{26} \times molarity$.

L_0 is the low frequency limit of the coupling coefficient which can be determined by experiments as done by Li et al. (1995) and expressed as

$$L_0 = -\frac{\phi}{\alpha_\infty}\frac{\varepsilon_f \varsigma}{\eta}\left[1 - a\alpha_\infty\frac{\widetilde{d}}{\Lambda}\right], \tag{2.5}$$

where ς is the zeta potential on the slipping plane and a is a constant assumed to be 2 in my calculation. Pride and Morgan (1991) find an expression for ς based on experiments as follows,

$$\varsigma = 0.008 + 0.026\log_{10}(C), \tag{2.6}$$

where C is the molarity of the solution. In the simulation, the electrolyte conductivity is $0.01S/m$, which is the same as what we use in the laboratory experiment.

In our numerical simulation, the L value is calculated by using a porous formation with the medium parameters listed in the Table 1.

Table 1: Medium properties used in the calculation of the coupling coefficient L.

	Porosity (%)	Ks (GPa)	Solid density (kg/m^3)	Solid Vp (m/s)	Solid Vs (m/s)	Permeability (darcy)
Formation	20	35	2600	2000	1200	0.1
Pore fluid density = 1000(kg/m^3)			Pore fluid viscosity = 0.001 Pa .S			
Pore fluid permittivity =80ε_0 (vacuum permittivity)			Formation permittivity =4ε_0 (vacuum permittivity)			

Taking the divergence of Eq. (2.1) and using $E=-\nabla\phi$ with generalized Ampere's law, we could obtain

$$\nabla^2\phi=\frac{L}{\sigma}(-\nabla^2 p+\omega^2\rho_f\nabla^2\varphi), \tag{2.7}$$

where φ is the displacement potential of the gradient field. To solve the equation (2.3) in the wavenumber domain, we get

$$\phi=A\cdot K_n(kr)+\frac{L}{\sigma}(-p+\omega^2\rho_f\varphi), \tag{2.8}$$

where k is the axial wavenumber, $Kn(kr)$ is the modified Bessel function of nth order and A is unknown coefficient for the electric field to be decided by the electric boundary conditions.

In the LWD geometry, using the expression of the displacement potentials in the elastic formation which is the 4th layer can be expressed as [11]:

$$\phi_4=B_4 K_n(kp_4r), \tag{2.9a}$$

$$\chi_4=D_4 K_n(ks_4r), \tag{2.9b}$$

$$\Gamma_4=F_4 K_n(ks_4r), \tag{2.9c}$$

and the displacement potential ϕ_4 is the φ in Eqs. (2.7) and (2.8), which is the compressional wave potential of the formation. χ_4 and Γ_4 are vertically and horizontally polarized shear wave potential of the formation. In terms of potentials, the radial displacement component u_r in the elastic formation can be expressed as:

$$u_r=\frac{\partial\phi_4}{\partial r}+\frac{1}{r}\frac{\partial\chi_4}{\partial\theta}+\frac{\partial^2\Gamma_4}{\partial r\partial z}. \tag{2.10}$$

Combining (2.9) and (2.10), we can get

$$u_r=B_4 K_n'(kp_4r)+\frac{n}{r}D_4 K_n(ks_4r)+iks_4F_4K_n'(ks_4r). \tag{2.11}$$

Substituting (2.9) into (2.8) and (2.10) into (2.1), we can get the expression for the potential ϕ_{wall}, radial strength E_{rwall} and the streaming current density J_{wall} of electric field along

the elastic borehole wall

$$\phi_{wall} = AK_n(kr) + (L/\sigma_{formation})\omega^2\rho_f B_4 K_n(kp_4 r), \tag{2.12a}$$

$$E_{rwall} = \frac{-\partial\phi_{wall}}{\partial r} = -AK_n'(kr) - (L/\sigma_{formation})\omega^2\rho_f B_4 K_n'(kp_4 r), \tag{2.12b}$$

$$J_{wall} = -\sigma_{formation} AK_n'(kr) + L\omega^2\rho_f \left[\frac{n}{r}D_4 K_n(ks_4 r) + iks_4 F_4 K_n'(ks_4 r)\right]. \tag{2.12c}$$

Under the quasi-static assumption, the electric field in the borehole satisfies the Laplace's equation [3], the solution for the potential ϕ_{flu}, radial strength E_{rflu} and the streaming current density J_{flu} is

$$\phi_{flu} = BI_n(kr) + CK_n(kr), \tag{2.13a}$$

$$E_{rflu} = \frac{-\partial\phi_{flu}}{\partial r} = -BI_n'(kr) - CK_n'(kr), \tag{2.13b}$$

$$J_{flu} = -\sigma_{flu}\frac{\partial\phi_{flu}}{\partial r} = -\sigma_{flu}\left[BI_n'(kr) + CK_n'(kr)\right], \tag{2.13c}$$

where B and C are the coefficients to be decided by the electric boundary conditions as well.

2.2 Boundary conditions in the LWD seismoelectric conversion

To solve the three coefficients A, B and C in the above expressions for the converted electric fields along the borehole wall (Eq. (2.12)) and in the borehole fluid (Eq. (2.13)), we apply the following three boundary conditions.

For acoustic boundary conditions, we have the continuity of the radial displacement u and stress element σ_{rr}, and the vanishing of the other two shear stress elements $\sigma_{r\theta}$ and σ_{rz}. For the electric boundary conditions, we have $\phi_{wall} = \phi_{flu}$, $J_{wall} = J_{flu}$ at the borehole wall, and the radial current density or the radial electric field strength (since they only differ in the multiplication of a conductivity) is equal to zero at the tool surface. At the tool surface, no current flowing between borehole fluid and tool surface. Thus, the radial current density or equivalently radial electric field strength should be set to zero.

2.3 Synthetic waveforms of LWD acoustic and seismoelectric signal

The formation properties are the same as the lab formation. A scaling factor of 17 is used to scale the lab tool to the real LWD tool. The source wavelet in the experiment is a square wave with a center frequency of 100 kHz. Scaling the 100kHz center frequency to the modeling, we use a Ricker wavelet with the center frequency of 6kHz as a source. The formulae in both acoustic and electric calculations are expressed in the wavenumber domain, thus we use the discrete wavenumber method [1] to do the modeling.

Figs. 1 and 2 show the calculated monopole and dipole waveforms using the formation parameters of our lab experiment. Solid curves are the acoustic signals and the
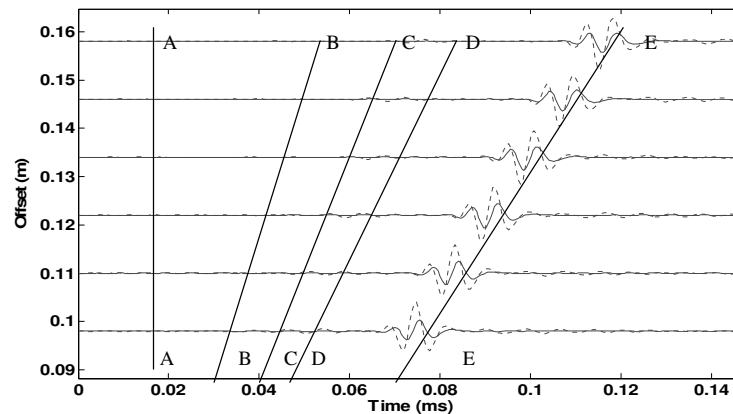
Figure 1: The monopole waveforms of the normalized acoustic pressure (solid curves) and the normalized electric field strength (dotted curves) for laboratory fast formation (A, B, C, D, E indicate the different arrivals described in the text).
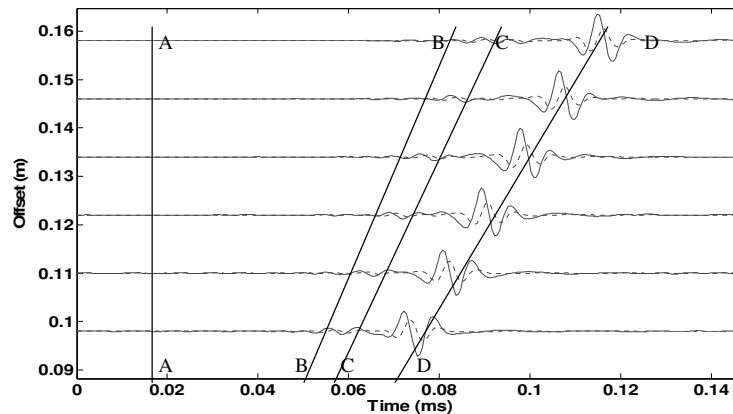

Figure 2: The dipole waveforms of the normalized acoustic pressure (solid curves) and the normalized electric field strength (dotted curves) for laboratory fast formation (A, B, C, D indicate the different arrivals described in the text).

dotted curves are the electric signals. (A-A) is the radiating electromagnetic wave in both figures. The figures are scaled back to the real lab borehole tool scale with the first trace located at $z = 0.098$m and the spacing is 0.012m.

In Fig. 1, (B-B) is the formation compressional wave, (C-C) is the monopole tool wave and (D-D) represents the formation shear wave, (E-E) is the Stoneley wave. We use the same semblance method to analyze the wave modes in the acoustic and electric waveforms as we did for the experiment data. The time domain semblances for the monopole acoustic and electric waveforms are shown in Figs. 3 and 4 respectively. The absence of the monopole tool mode which is indicated by the first big block in Fig. 3 can be observed very clearly in the semblance of the electric signal (Fig. 4).
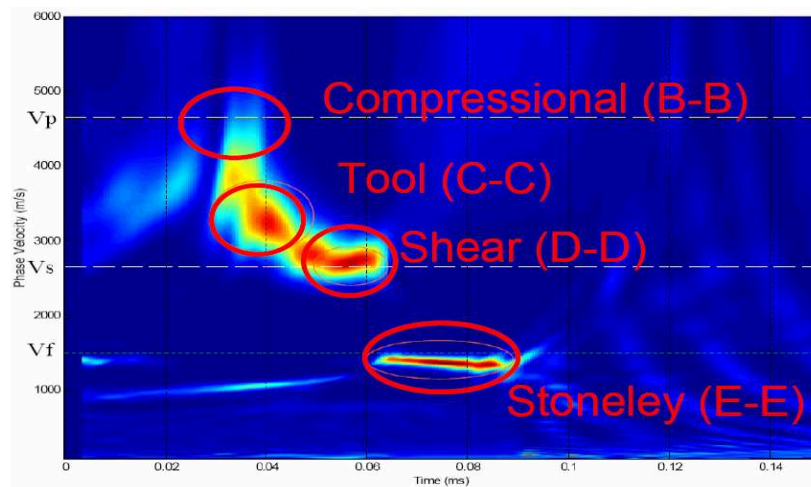
Figure 3: The time domain semblance of the monopole acoustic waveforms in Fig. 7. (The three circles indicates the monopole tool wave, shear wave and stonely wave respectively from top to bottom. Compressional wave is not very clear in this figure. Vp stands for the formation P wave velocity, Vs for S wave velocity, Vf for fluid wave velocity.)
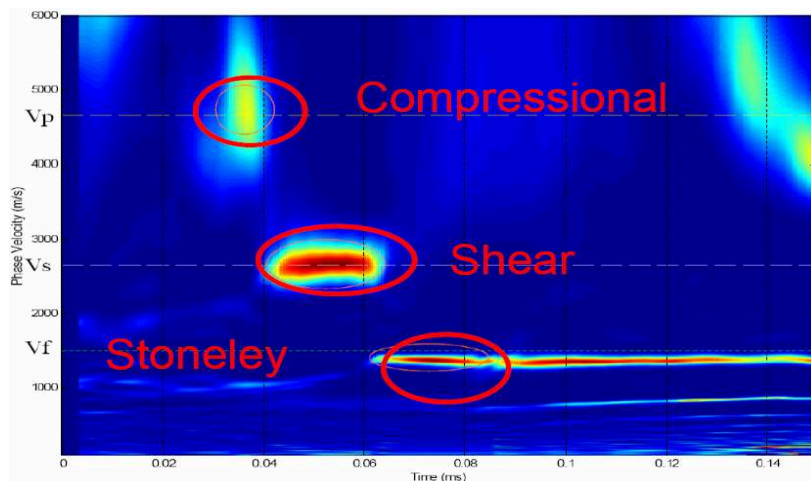

Figure 4: The time domain semblance of the monopole electric waveforms in Fig. 7. (The three circles indicates the monopole compressional wave, shear wave and stonely wave respectively from the top to bottom. Vp stands for the formation P wave velocity, Vs for S wave velocity, Vf for fluid wave velocity.)

The same phenomena can be observed for the dipole case. In Fig. 2 (B-B), (C-C), (D-D) are the 2nd order dipole formation flexural wave, dipole tool wave and 1st order dipole formation flexural wave, respectively. The absence of the dipole tool mode, which is indicated by the second big block in Fig. 5, can be observed very clearly in the semblance of the electric signal (Fig. 6).
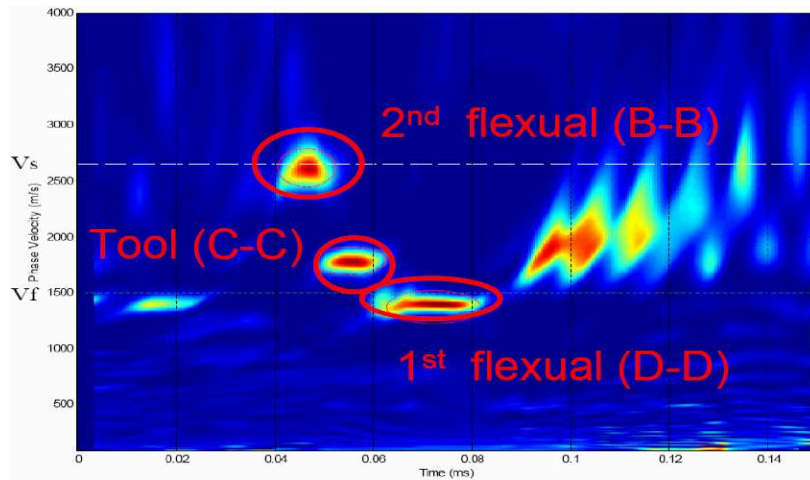
Figure 5: The time domain semblance of the dipole acoustic waveforms in Fig. 8. (The three circles indicates the 1st order dipole formation flexural wave, tool wave and 2nd order formation flexuraly wave respectively from the above to the bottom. Vs stands for formation S wave velocity. Vf for fluid wave velocity.)

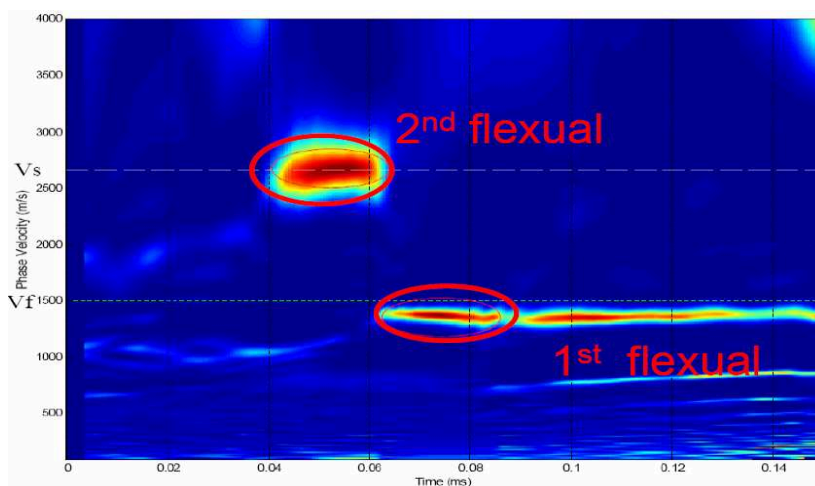Figure 6: The time domain semblance of the dipole electric waveforms in Fig. 8. (The two circles indicates the 1st order dipole formation flexural wave and 2nd order formation flexural wave respectively from the above to the bottom. Vs stands for formation S wave velocity, Vf for fluid wave velocity.)

3 Laboratory experiments

To simulate the LWD measurement, we built a scaled multipole acoustic tool composed of three parts: the source, receiver, and a connector [13]. Working in the ultrasonic frequencies the tool is put into a scaled borehole to measure the monopole and dipole acoustic waves. For the seismoelectric measurements, we only need to change the receiver section from the acoustic transducer array to the electrode array with the same spacing and lo-

cated at exactly the same location. Thus, we could measure the LWD acoustic and electric signal generated from the same acoustic source approximately along the same path.

3.1 Experimental borehole model

The experiment borehole model we use is a homogenous, isotropic sandstone block with a length of 30cm, a width of 29cm, and a height of 23cm. The porosity of sandstone is about 20% and permeability is about 50 millidarcy. Borehole diameter is 1.7cm. All velocities are shown in Table 2. Schematics of the LWD borehole model is shown in Fig. 7.

Table 2: LWD laboratory borehole model parameters.

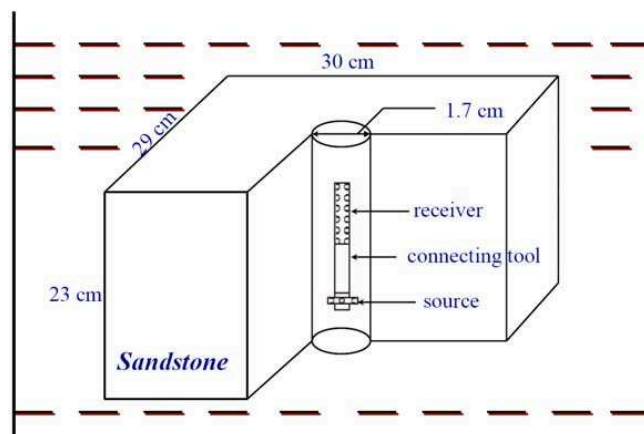|	P-velocity	S-velocity	Density	Outer Radius
Inner Fluid	1500 m/s	——	1000 kg/m^3	0.002 m
Tool (Composite)	5800 m/s	3100 m/s	7700 kg/m^3	0.005 m
Outer Fluid	1500 m/s	——	1000 kg/m^3	0.0085 m
Formation	4660 m/s	2640 m/s	2100 kg/m^3	∞

Figure 7: Schematics of the borehole model in the laboratory measurement.

3.2 Structure of LWD multiple tool for acoustic and seismoelectric measurements

Our laboratory LWD tool includes three sections: the source, the receivers, and the connector. Both the source and receiver acoustic transducers are made of PZT crystal disks of 0.635cm in diameter and 0.37cm in thickness. The dimension of the tool is shown in Fig. 8. For the scaled LWD tool, we use the equivalent composite tool velocity to indicate
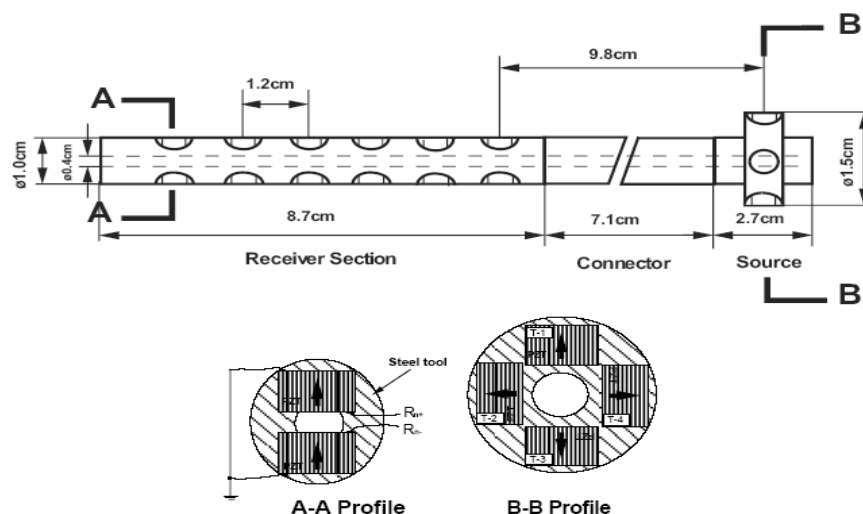
Figure 8: Schematic diagram of the scaled lab multipole tool in LWD acoustic measurement. The arrows indicate the polarization of the PZT disks [13].

the steel tool has holes in it to embed acoustic transducers and electrodes. The tool ID is 0.4cm, OD is 1cm.

The source is made of four separate crystal disks shown in the B-B profile of Fig. 8. The arrows on the disks indicate their piezoelectric polarization. The receiver section is composed of six pairs of crystal disks at six different locations. The polarizations of each disk pair are shown in the A-A profile of Fig. 8. By changing the electric polarization of the source PZT disks and by combining the signals received by the receiver pairs, we are able to simulate a working system of acoustic logging sources. To measure the seismoelectric signal, we need to change the receiver section from acoustic transducers to electrodes. The electrodes used for this experiment are point electrodes of 1.0mm in diameter. Thus, each electrode on the electrode array can only detect the electric field around it.

3.3   LWD acoustic and seismoelectric signals in the sandstone borehole

It is generally accepted that the electric double layer (EDL) is the basis for the electroki-netic conversion [5, 8]. For our sandstone borehole model, an EDL is developed at the borehole formation — borehole fluid interface and inside porous formation. When the acoustic waves propagate along the borehole wall, a localized electric field is generated and the electrode detects this electric field. Since the conductivity of the borehole fluid is low, the recorded voltage between the electrode and ground can represent the electric field generated at the borehole. The difference between rock and steel tool is that the latter one is a conductor. By effectively grounding of the drilling collar during the real LWD process, there could be no excess charge accumulation at steel tool surface. Though

tool waves propagate along the rigid tool surface with large amplitude, no excess charge can be moved by the tool wave pressure to induce a localized electric field at the tool — borehole fluid interface. Thus, in the seismoelectric signals, what we record are purely the electric fields excited by the acoustic waves propagating in the borehole formation and with the velocities of formation acoustic modes.

We first calibrate our experimental transducer with a standard transducer, whose frequency response is well determined by manufacture. The maximum acoustic pressure generated from our lab size transducer is about $450Pa$. In the laboratory experiments, we need to use small acoustic transducers to fit in our lab tool and borehole as indicated by Figs. 9 and 10. Given the coupling coefficient theoretically computed in Section 2, and electrolyte conductivity to be $0.01S/m$, the maximum amplitude of converted seismoelectric signals in the time domain waveforms is about 0.45mv.

We now examine the two kinds of signals for monopole (Fig. 9) and dipole (Fig. 10) excitations using time domain analysis. From the acoustic waveform we can clearly see a monopole tool wave coming between P and S wave and a low frequency dipole tool wave coming in the late part of the wave train. In the time domain semblance we can observe the peaks at the monopole and dipole tool waves. In the seismoelectric data, tool modes do not exist. Of course, the velocity of the tool modes may slightly change due to the borehole environment. These results show that by measuring the seismoelectric signal during the logging-while-drilling process, we can potentially eliminate tool modes.

Based on the laboratory experiments we conclude the following:

    LWD acoustic signal = Formation acoustic waves + Tool waves + Noise,
    LWD SEL signal = Formation acoustic wave induced electric signals + Noise.

In field acoustic LWD operation, tool modes velocities could be close to formation velocities in some formations. Therefore, detection of formation arrivals can be hampered by tool mode contamination. LWD seismoelectric signals do not contain tool mode induced electric signals. We measure the similarity between the acoustic and SE signals using their respective spectra. There are several reasons for this to be done in the frequency domain instead of the time domain. 1) In the frequency range where the formation acoustic wave modes exist, the waveforms overlap better. In other frequency ranges where the waveforms differ greatly due to the different modes content, it is difficult to find the correlation between the two signals. 2) There are phase difference between the two signals due to the various circuit elements used in laboratory collection of the two signals and the seismoelectric coupling. 3) In the acoustic record, it takes time for the main acoustic energy to propagate from the borehole wall to the receiver transducer at the fluid acoustic velocity. While the propagation time for the electric signal can be ignored due to the high EM wave speed. Thus, it is more difficult to compare the two signals in time domain than in the frequency domain.
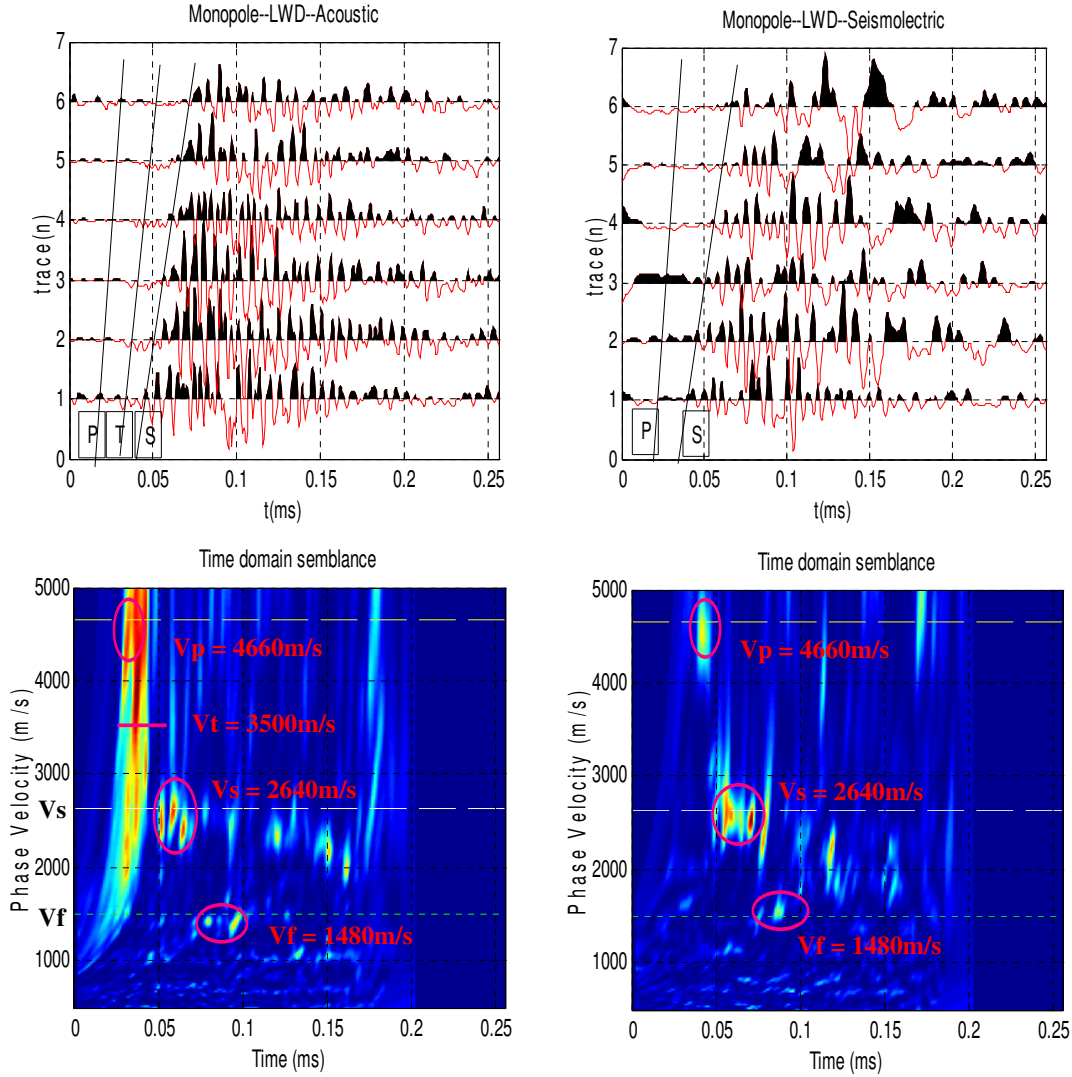
Figure 9: Monopole LWD acoustic (left) and seismoelectric signal (right) comparison. (Vp stands for formation P wave velocity, Vs for formation S wave velocity, and Vf for fluid velocity; Vt for tool wave velocity, P means P wave, S means S wave, T means tool wave.)

We calculate the similarity coefficients of the two signals defined by

$$r = \frac{\sum\limits_{m} A_m B_m}{\sqrt{\sum\limits_{m}(A_m)^2 (B_m)^2}},$$

(3.1)

where A_m and B_m are the acoustic and electric amplitude spectrum, m is the index of the sampling point in frequency domain. A moving window is used to scan the spectra of
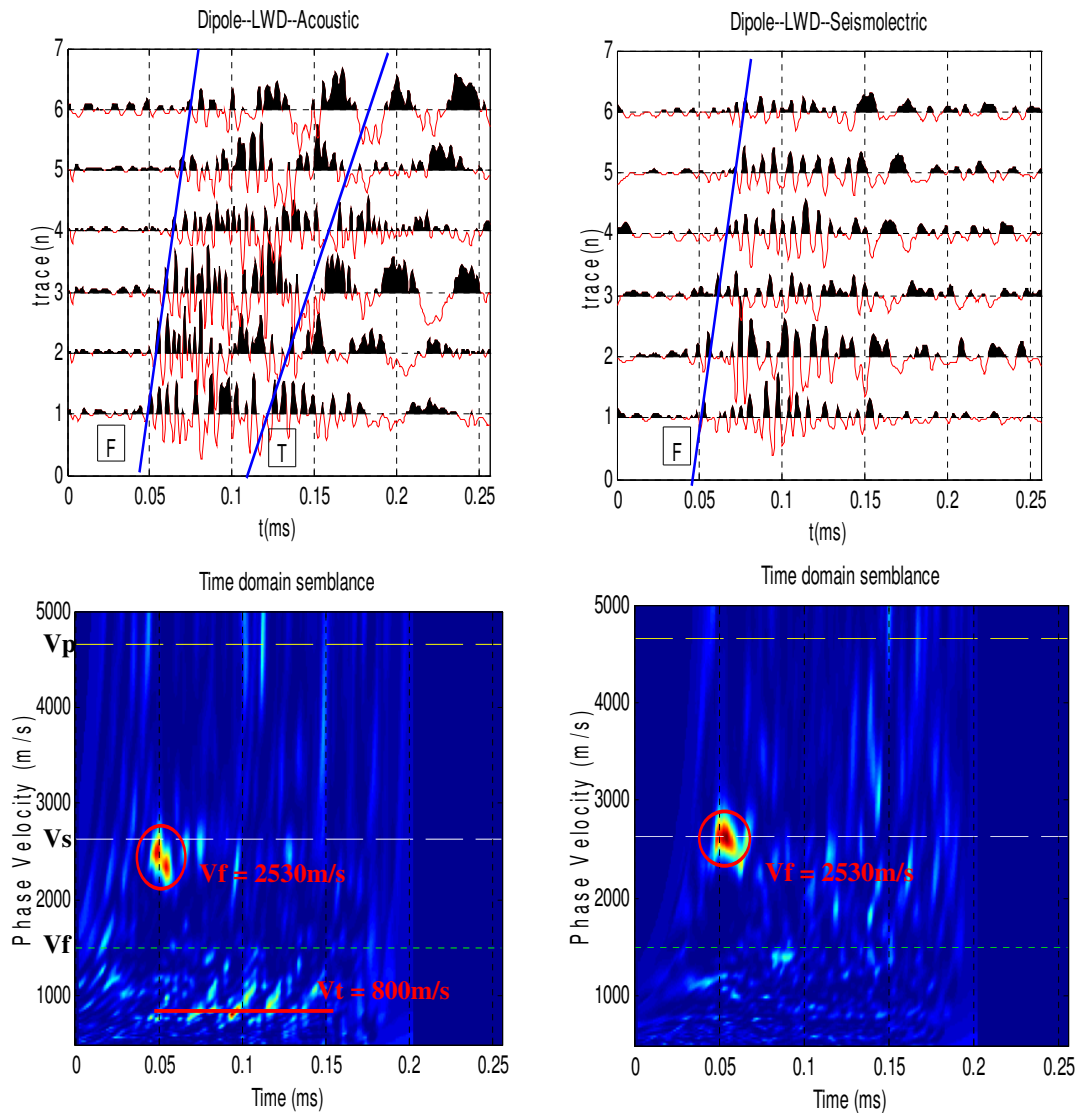
Figure 10: Dipole LWD acoustic (left) and seismoelectric signal (right) comparison. (Vf stands for flexural wave velocity, Vt for tool wave velocity; F means formation flexure wave, T means tool wave.)

the two signals simultaneously. The similarity coefficient of that window is set to be the similarity for the center frequency of the window.

The similarity curves and the filtered results are shown in Fig. 11 for monopole excitation and Fig. 12 for dipole excitation. In Fig. 11, ST stands for Stoneley wave, T stands for monopole tool wave. In Fig. 12, F stands for dipole flexural wave, T stands for dipole tool wave. The monopole similarity curve is similar to a band stop filter. The dipole coherence curve is similar to a band pass filter.
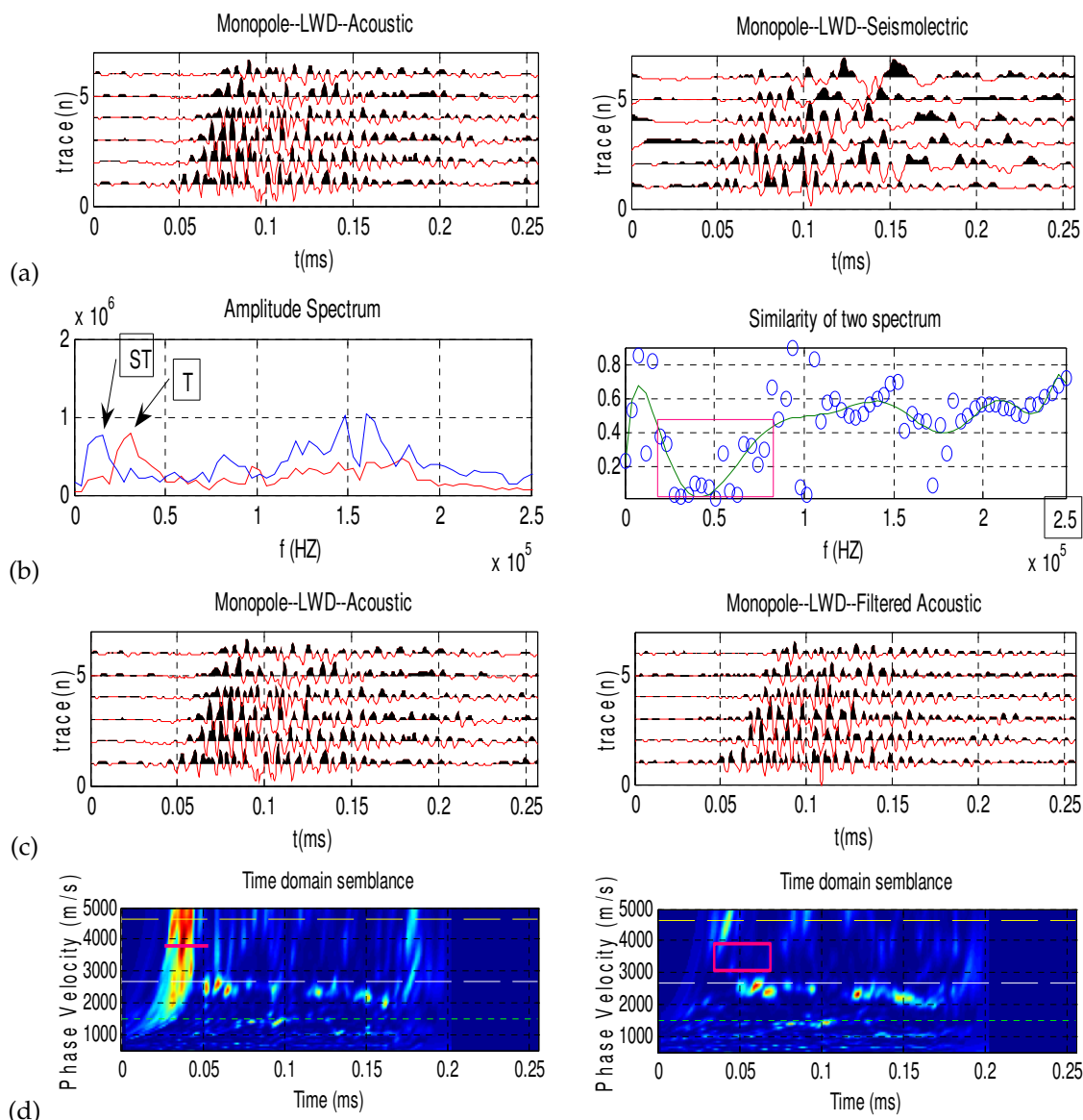
Figure 11: (a) Monopole acoustic (left) and seismoelectric (right) waveforms; (b) monopole acoustic (line with arrow "T") and seismoelectric (line with arrow "ST"). Fourier amplitude spectra (left) and coherence as a function of frequencies (right); (c) monopole unfiltered acoustic (left) and filtered (right) waveforms; and (d) their time domain semblances. (T means frequency peak due to tool wave, ST stands for Stoneley wave).

After obtaining a coherence curve (Fig. 11b right, Fig. 12b right), we use it to design a zero-phase filter to be applied to the acoustic signal. A time domain semblance for the filtered data is then computed. We can see clearly that the filtered data contains only formation acoustic modes (Fig. 11c right, Fig. 12c right). Other benefits of this filtering
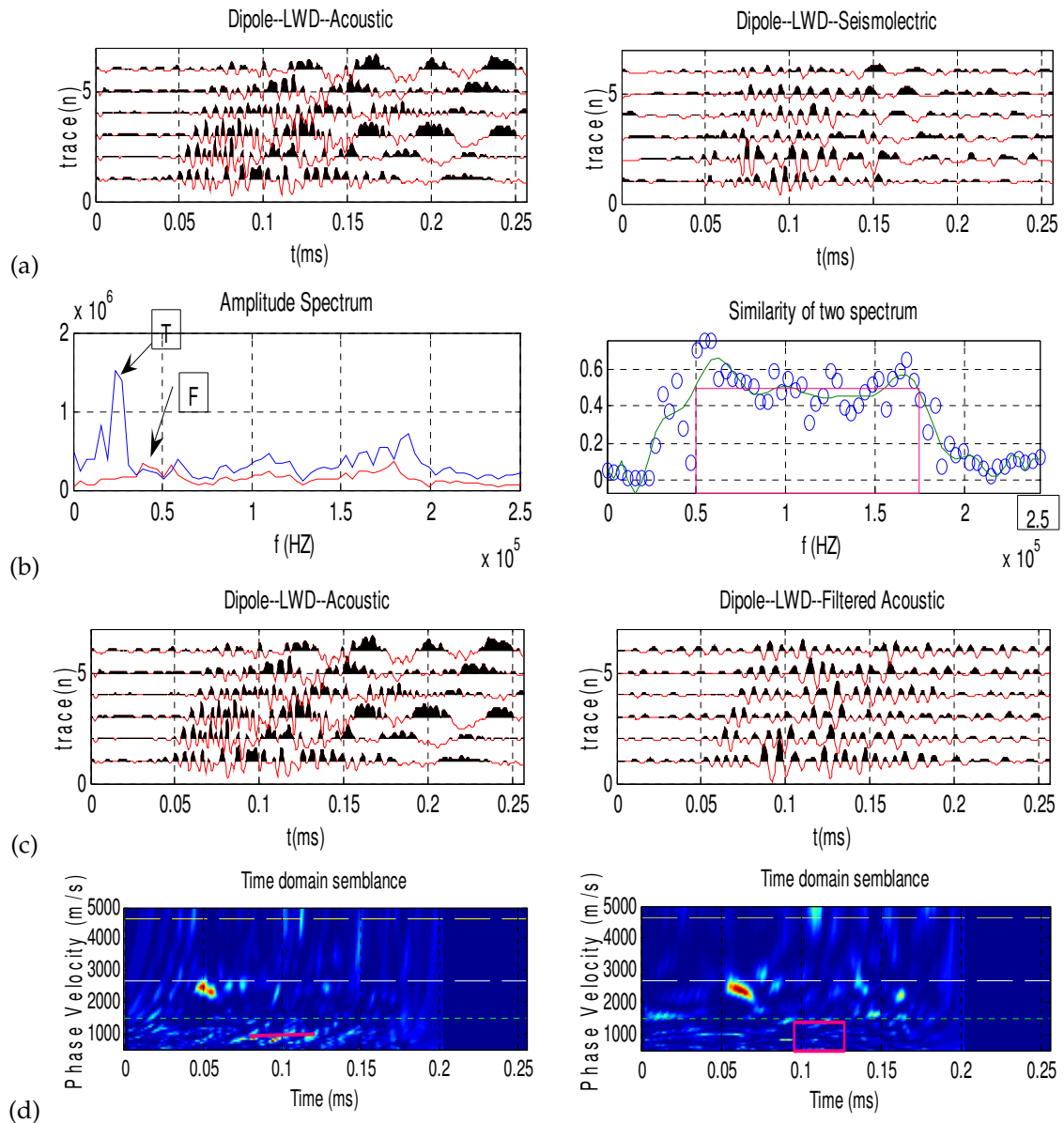
Figure 12: (a) Dipole acoustic (left) and seismoelectric (right) waveforms; (b) dipole acoustic (line with arrow "T") and seismoelectric (line with arrow "F") Fourier amplitude spectra (left) and coherence as a function of frequencies (right); (c) dipole unfiltered acoustic (left) and filtered (right) waveforms; and (d) their time domain semblances. (T means frequency peak due to tool wave, F stands for Flexural wave).

method include the reduction of noise in the acoustic signal as well. To further demonstrate these benefits, we detect the peaks in the acoustic and seismoelectric signal spectra and calculate the corresponding wave velocity of those frequency peaks. We find that

in the frequency range with low similarity the wave velocities are also different, which means the wave modes are different.

The above analysis illustrates that by correlating the LWD seismoelectric signal with the acoustic signal, we can pick out formation acoustic modes from the LWD acoustic measurement and reduce the noise. This is a very significant result for extracting the formation arrivals from real-time LWD field data that may be contaminated by the complex tool modes and the drilling noise.

4   Conclusions and discussions

In this paper, we studied the electric fields induced by borehole monopole and dipole LWD acoustic waves both theoretically and experimentally. A Pride-theory-based model for the acoustic wave induced electric field in the LWD geometry can also be used to calculate the electric field strength excited by the acoustic pressure. We also developed laboratory experimental set-up and procedures as well as processing methods to enhance the recorded seismoelectric signal. A suite of acoustic and seismoelectric measurements are made to demonstrate and understand the mechanism of the borehole seismoelectric phenomena, especially under LWD acoustic excitation.

Summarizing the whole paper, the following two conclusions can be reached: 1. LWD seismoelectric signals do not contain contributions from tool modes. 2. By correlating the LWD seismoelectric and acoustic signals, we can effectively separate the real acoustic modes from the tool modes and improve the overall signal to noise ratio in acoustic LWD data.

Laboratory experiments with good control of noise level and medium salinity brines are ideal settings compared to the field measurements. In practice, during drilling, a pressure difference between formation and borehole creates mud invasion and pressure transients can also generate seismoelectric signals. In well drilled with oil-based mud, seismoelectric potential will also exist if the mud contains a water fraction. In the case of bottom hole pressure to be a few *kpsi*, streaming potential signal could be at the order of tens of *mv*. This indicates the feasibility of collecting seismoelectric signal in real drilling environment.

This paper has taken the first step towards understanding borehole LWD seismoelectric phenomena. With future improvements in both theory and instrumentation, seismoelectric LWD might evolve into a new logging method in the future.

Acknowledgments

References

[1] Bouchon, M. (2003). A review of the discrete wavenumber method. Pure and Applied Geophysics. 160, 445-465.

[2] Cittá, F., Russell, C., Deady, R., and Hinz D. (2004). Deepwater hazard avoidance in a large top-hole section using LWD acoustic data. The Leading Edge, 23, 566-573.

[3] Hu, H. S. and Liu, J. Q. (2002). Simulation of the converted electric field during acousto-electric logging. SEG Int'l Exposition and 72nd Annual Meeting, Salt Lake City, Utah, 2002, October 6-11.

[4] Joyce, B., Patterson, D., Leggett, J. V., and Dubinsky, V. (2001). Introduction of a new omni-directional acoustic system for improved real-time LWD sonic logging-tool design and field test results. SPWLA 42nd Annual Logging Symposium.

[5] Loren, B., Perrier, F., and Avouac, J. P. (1999). Streaming potential measurements 1. Properties of the electrical double layer from crusted rock samples. J. Geophys Res., 104, 17857-17877.

[6] Market, J., Althoff, G., Barnett, C., and Deady, R. (2002). Processing and quality control of LWD dipole sonic measurements. SPWLA 43rd Annual Logging Symposium, Osio, Japan.

[7] Mikhailov, O. V. (1998). Borehole Electroseismic Phenomena. Ph.D. Thesis, Massachusetts Institute of Technology, Department of Earth, Atmospheric and Planetary Sciences.

[8] Pride, S. R. and Morgan, R. D. (1991). Electrokinetic dissipation induced by seismic waves. Geophysics, 56, 914-925.

[9] Pride, S. R. (1994). Governing equations for the coupled electromagnetics and acoustics of porous media. Phys. Rev. B, 50, 15678-15696.

[10] Pride, S. R. and Haartsen, M. W. (1996). Electroseismic wave properties. J. Acoust. Soc. Am., 100, 1301-1315.

[11] Zhan, X. (2005). A Study of Seismoelectric Signals in Measurement While Drilling. MSc. Thesis, MIT.

[12] Zhu, Z. and Toksöz, M. N. (1998). Seismoelectric and seismomagnetic measurements in fractured borehole models. In Expanded Abstract, 69th Ann. Internat. Mtg., pages 144-147. Soc. Expl. Geophys.

[13] Zhu, Z., Rao, V. N. R., and Burns, D. R., and Toksöz, M. N. (2004). Experimental studies of multipole logging with scaled borehole models. Borehole Acoustic and Logging / Reservoir Delineation Consortia Annual Report, MIT.